NEUROPHYSIOLOGY

3D architecture and a bicellular mechanism of touch detection in mechanosensory corpuscle

Yury A. Nikolaev[1]†, Luke H. Ziolkowski[1]†, Song Pang[2]‡, Wei-Ping Li[2], Viktor V. Feketa[1,3], C. Shan Xu[2]§, Elena O. Gracheva[1,3,4,5]*, Sviatoslav N. Bagriantsev[1]*

Mechanosensory corpuscles detect transient touch and vibration in the skin of vertebrates, enabling precise sensation of the physical environment. The corpuscle contains a mechanoreceptor afferent surrounded by lamellar cells (LCs), but corpuscular ultrastructure and the role of LCs in touch detection are unknown. We report the three-dimensional architecture of the avian Meissner (Grandry) corpuscle acquired using enhanced focused ion beam scanning electron microscopy and machine learning-based segmentation. The corpuscle comprises a stack of LCs interdigitated with terminal endings from two afferents. Simultaneous electrophysiological recordings from both cell types revealed that mechanosensitive LCs use calcium influx to trigger action potentials in the afferent and thus serve as physiological touch sensors in the skin. The elaborate architecture and bicellular sensory mechanism in the corpuscles, which comprises the afferents and LCs, create the capacity for nuanced encoding of the submodalities of touch.

INTRODUCTION

The sense of touch is essential for handling objects and tools, foraging, navigating an environment, and forming social bonds (*1*). In vertebrates, the various properties of touch are detected in the skin by mechanosensory corpuscles and hair follicle-associated lanceolate complexes (*2*, *3*). Although morphologically and functionally diverse, these end organs invariably contain terminal Schwann cells (TSC) that form close interactions with mechanoreceptor afferent terminals. The afferents, which express mechanically gated ion channels such as Piezo2 (*4*, *5*), are considered to be the only touch-sensing elements within these end organs, but recent work has revealed that dissociated mouse Schwann cells display mechanosensitivity in culture (*6*, *7*). Moreover, mammalian Meissner corpuscles and their avian analogs (historically called corpuscles of Grandry and referred to here as avian Meissner corpuscles) contain TSCs known as lamellar cells (LCs) (*8*, *9*), which fire mechanically activated action potentials (APs) in intact avian Meissner corpuscles in situ (*10*). These studies suggest that the sensory afferent may not be the sole sensory element and that LCs could be additional physiological sensors of touch in diverse vertebrates. However, the detailed architecture of LC-afferent complexes is unknown. Thus, the role of LCs remains speculative in the absence of structural and functional insight into the relationship between LCs and sensory afferents (*11*).

[1]Department of Cellular and Molecular Physiology, Yale University School of Medicine, New Haven, CT 06510, USA. [2]Janelia Research Campus, Howard Hughes Medical Institute, Ashburn, VA 20147, USA. [3]Department of Neuroscience, Yale University School of Medicine, New Haven, CT 06510, USA. [4]Program in Cellular Neuroscience, Neurodegeneration and Repair, Yale University School of Medicine, New Haven, CT 06510, USA. [5]Kavli Institute for Neuroscience, Yale University School of Medicine, New Haven, CT 06510, USA.
*Corresponding author. Email: elena.gracheva@yale.edu (E.G.); slav.bagriantsev@yale.edu (S.B.)
†These authors contributed equally to this work.
‡Present address: Yale University School of Medicine, New Haven, CT 06510, USA.
§Present address: Department of Cellular and Molecular Physiology, Yale University School of Medicine, New Haven, CT 06510, USA.

RESULTS

Architecture of avian Meissner corpuscles

To determine the detailed structure of a Meissner corpuscle, we used focused ion beam scanning electron microscopy (FIB-SEM) to image bill skin from a tactile foraging Mallard duck (*Anas platyrhynchos domesticus*). We scanned a volume of 47,250 μm^3, comprising 4753 consecutive images at a voxel size of 8 × 8 × 8 nm, and used machine learning to reconstruct the three-dimensional (3D) architecture of an entire LC-afferent complex and its associated structures. The boundary box for reconstruction had dimensions of 35 μm by 45 μm by 30 μm, of which, the corpuscle occupied a volume of 8167 μm^3 (Fig. 1A and table S1).

The outer layer of the corpuscle, formed by satellite cells and collagen fibers, encapsulates a sensory core comprising a stack of six LCs (LC1 to LC6) innervated by two afferents (Fig. 1, B to D, and movies S1 and S2). Both afferents are covered with myelinating Schwann cells outside the corpuscles (Fig. 1, B and C). Afferent 1 interdigitates with the LCs, forming disk-like endings that cover up to 42% of the apposing surfaces of LC1 to LC6 (Fig. 1, D and E, and fig. S1). The discoid endings form protrusions that extend around LC1 (Fig. 1E). Afferent 2 forms a single, smaller, ovoid ending between LC5 and LC6 and covers 16% of the lower surface of LC6 (Fig. 1, C to E, and fig. S1). One of the satellite cells, whose cell body was outside of the afferent-LC core, formed fine projections interleaved between afferent 2 and LC5 (fig. S2). We reconstructed the LC-afferent core of another corpuscle from the same skin volume, which contained a stack of three LCs. This corpuscle is innervated by a single afferent which, like afferent 2, formed a single disk in the LCs stack (fig. S3). Thus, avian Meissner corpuscles can be innervated by one or two afferents. The difference in the innervation pattern among the afferents indicates that they could be molecularly and physiologically distinct (*8*).

Structural coupling between lamellar and afferent membranes

Between the disk-shaped afferents, the six LCs form flattened structures, 6 to 9.6 μm thick and 23.9 to 33.1 μm along the longest

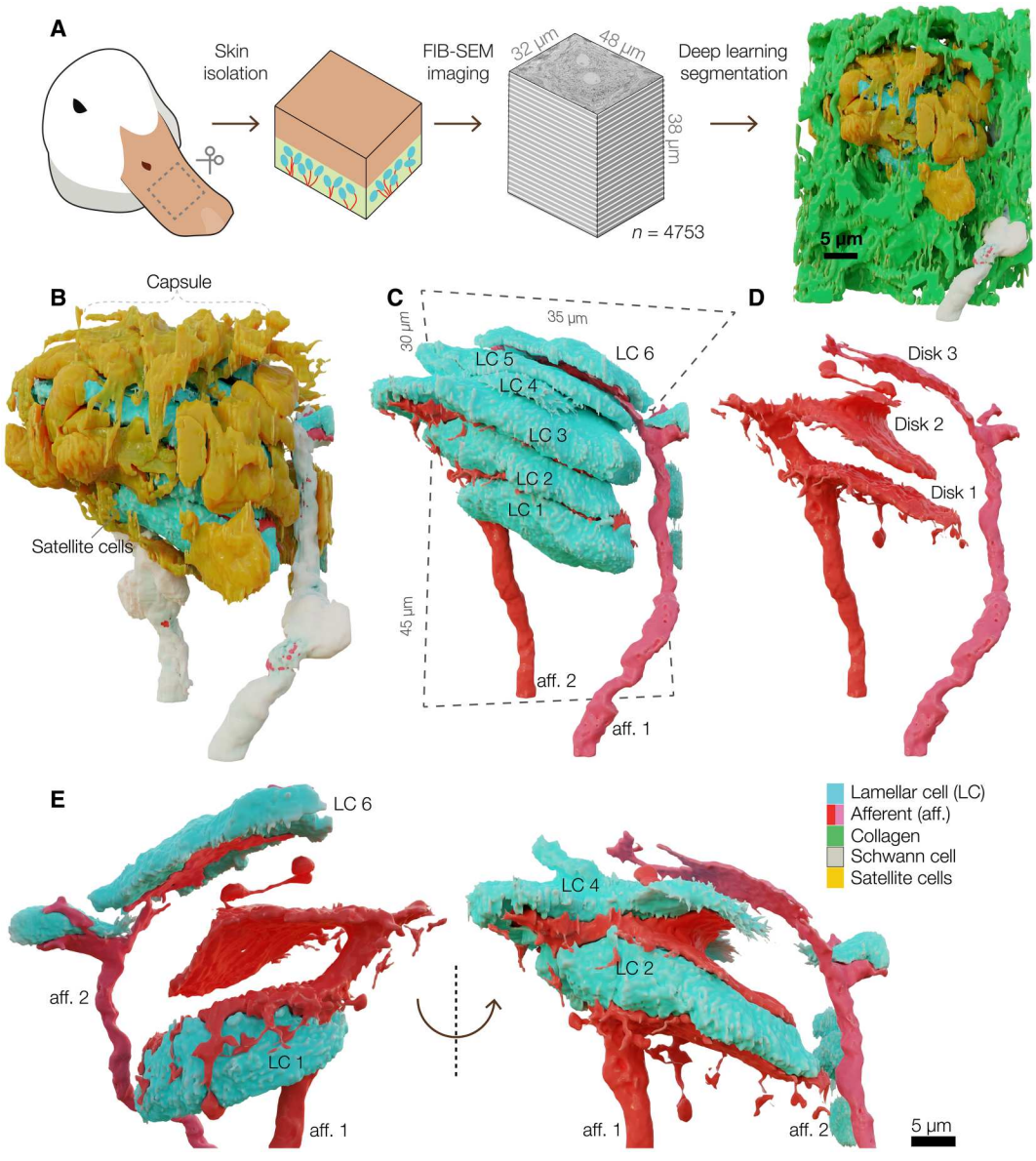

Fig. 1. Meissner corpuscles comprise a stack of LCs interdigitated with terminal afferent disks. (**A**) FIB-SEM workflow for automated segmentation and machine learning-based 3D reconstruction of a Meissner corpuscle in duck bill skin from 4753 SEM images. (**B** to **D**) Three-dimensional architecture of a Meissner corpuscle (B), corpuscle without outer capsule (C), isolated afferents (D). (**E**) Three-dimensional architecture of a section of afferent 1 and afferent 2 and associated LCs. aff., afferent.

dimension. Small villi protrude from the edges of each LC and form contacts with the surrounding satellite cells and collagen (Fig. 2, A and B). The cytosol of each LC contains 19,981 to 37,306 dense core vesicles (DCVs), ~150 nm in diameter, which occupy 2 to 3% of the volume of each LC (Fig. 2, B to E, and fig. S4). Approximately 1% of all DCVs were within 30 nm from the membrane facing the afferent, suggesting they could represent a readily releasable pool (Fig. 2F). We used transmission electron microscopy and electron tomography to reconstruct and segment a 3.16 µm by 2.16 µm by 0.25 µm box containing an LC-afferent disk contact (movies S3 and S4). High-resolution close-up reconstruction of a fragment of the LC-afferent contact area revealed that DCVs fuse with regions of the LC plasma membrane that appose the neuronal disk, suggesting that DCVs release their contents into the intermembrane space (Fig. 2, G and H, and movie S5). Densely coated membrane pits structurally resembling lipid raft structures called caveolae were also found adjacent to DCVs (Fig. 2, G and H, and movie S5). RNA sequencing of corpuscles extracted from bill skin revealed robust expression of components of DCV biogenesis and release, including soluble N-ethylmaleimide-sensitive-factor attachment protein receptor (SNARE) proteins, as well as mechanically gated and voltage-gated ion channels (fig. S5). This supports our observation of DCVs and earlier data showing that LCs are mechanosensitive and excitable (*10*).

Although the sensory afferent in the reconstruction contained smaller, clear vesicles, we did not detect clearly identifiable synapses, the typical sites of clear vesicle vision, between the LC and afferent plasma membranes. Instead, we found membrane densities

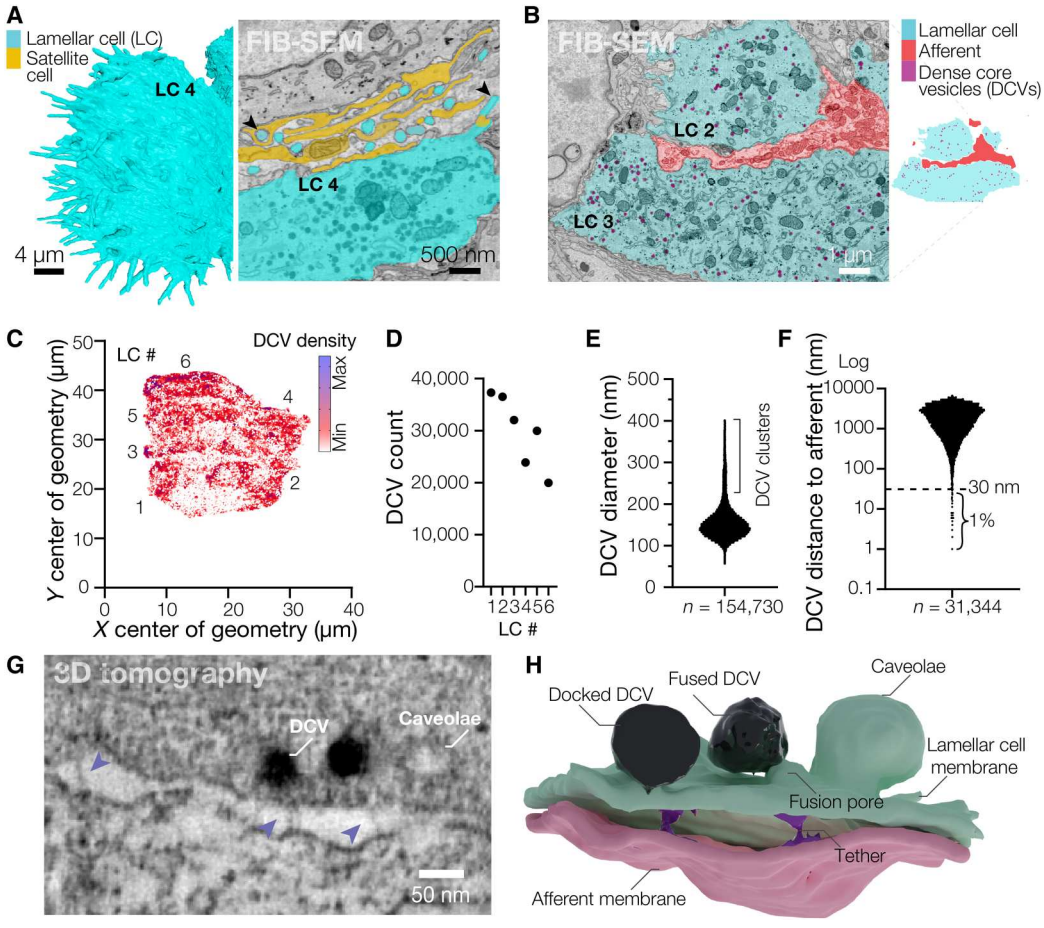

Fig. 2. Lamellar cells interact with the afferent via DCVs and tethers. (**A**) Close-up 3D reconstruction of villi protruding from the edge of LC4 and a pseudo-colored scanning electron microscope image of villi (black arrowheads) protruding from the edge of LC4 and contacting the satellite cell and afferent. (**B**) A pseudo-colored scanning electron microscope image depicting DCVs inside LCs (left) and a corresponding map of the cell types shown in the image (right). (**C**) A density map of DCVs in LCs. (**D** to **F**) Quantification of the total DCV count per LC (D), DCV diameter (E), and distance from each DCV to the closest afferent membrane (F). *n* is the total number of DCVs. (**G**) Transmission electron microscopy image of the LC-afferent contact area. Blue arrowheads point to tethers connecting LC and afferent plasma membranes. (**H**) Three-dimensional reconstruction of a fragment of the LC-afferent contact area.

resembling adherens junctions (movies S3 and S4). In addition, we observed 26- to 32-nm-long tethers connecting the membranes throughout the LC-afferent contact area, including at sites of DCV fusion (Fig. 2, G and H, and movie S5). Together with earlier data (*10*), these findings reveal that avian Meissner LCs are mechanosensitive secretory cells that form large contact areas with sensory afferents and tether-like connections with afferent membranes, suggesting a possible functional interaction between LCs and afferent terminals.

Functional coupling between mechanosensitive lamellar and the afferent

Because patch-clamp recordings directly from Meissner LCs in duck bill skin previously revealed that LCs are mechanosensitive (*10*), we sought to test the idea that LCs can induce firing in sensory afferents and thereby act as bona fide touch sensors. As a first step, we used a method for electrophysiological recordings of afferent nerve activity from a single corpuscle in duck bill skin during mechanical stimulation of the same corpuscle (Fig. 3A) (*12*). Mechanical stimulation of the corpuscle with a blunt glass probe mounted on a piezoelectric actuator evoked AP firing in the afferent (Fig. 3, B and C). APs occurred in a 1:1 correspondence with indentations during a 20-Hz vibratory stimulation (Fig. 3D), consistent with the role of avian Meissner corpuscles as detectors of transient touch and vibration (*9*, *13*, *14*). We detected two types of firing patterns in the afferent. In most cases, APs were triggered in a rapidly adapting fashion, i.e., only during the dynamic phases of the stimulus (Fig. 3E). However, 2 out of more than 50 recorded afferents showed slowly adapting firing (fig. S6). This supports our structural data showing two morphologically distinct afferents in the corpuscle and agrees with earlier findings in mice (*8*). Application of the voltage-gated sodium channel blocker tetrodotoxin suppressed AP generation, revealing low-amplitude receptor potentials (Fig. 3, B to D), consistent with the presence of mechanically gated ion channels in the afferent ending (*12*).

Mechanical stimulation of the corpuscle inevitably acts on both the afferent and LCs; therefore, to test whether activation of a single LC can trigger afferent firing, we selectively activated a single LC by whole-cell patch-clamp while simultaneously recording afferent activity from the same corpuscle with a second electrode (Fig. 4, A and

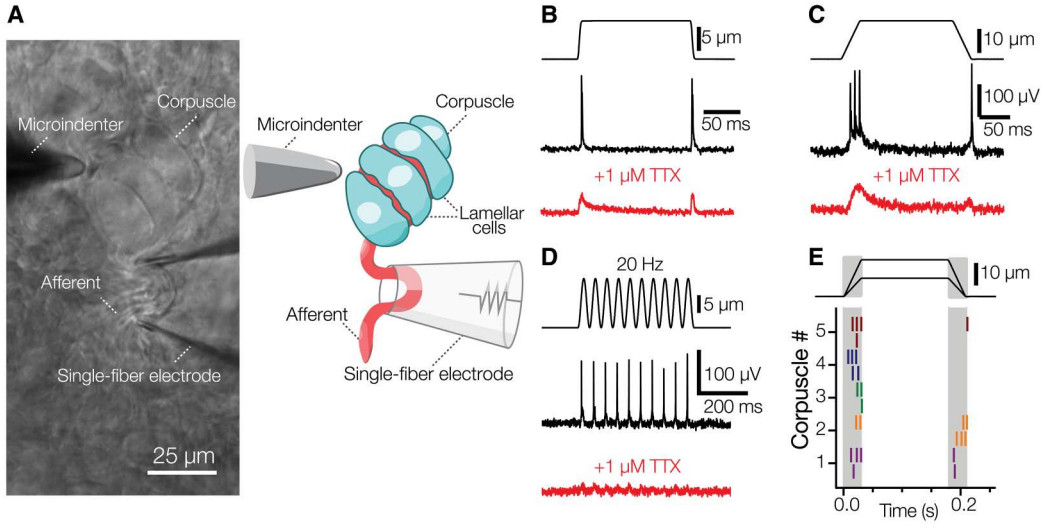

Fig. 3. Avian Meissner corpuscles detect transient touch. (**A**) A bright-field image and schematic representation of the experimental setup to record afferent activity from intact Meissner corpuscle in duck bill skin. (**B**) Mechanical step stimulus applied with a glass probe (top), representative rapidly adapting single-fiber response comprising APs (middle), and representative single-fiber response in the presence of 1 μM TTX (voltage-gated sodium channel blocker) comprising receptor potentials (bottom). (**C**) Mechanical step stimulus with long ramp phases (top), representative rapidly adapting single-fiber response comprising APs (middle), and representative single-fiber response in the presence of 1 μM TTX comprising receptor potentials (bottom). (**D**) Vibratory mechanical stimulus (top), representative single-fiber response comprising APs (middle), and representative single-fiber response in the presence of 1 μM TTX comprising receptor potentials (bottom). (**E**) Raster plot of rapidly adapting afferent firing for five different corpuscles in response to mechanical stimuli of two different indentation depths. Each vertical dash represents an individual AP. TTX, tetrodotoxin.

B). To our knowledge, such an experiment has not been performed for any tactile corpuscle in any species. When LCs were stimulated by depolarizing current injection in the current clamp mode, they displayed robust AP firing, as expected (*10*). Concurrent AP firing was also detected in the recorded afferents (Fig. 4, C and E). The waveforms in the afferent triggered by LC activation were indistinguishable from the waveforms triggered by mechanical stimulation of the corpuscle (fig. S7, A and B). Next, we tested if APs can be triggered in the afferent when LCs are activated by voltage-clamped depolarization to 0 mV with a potassium-based physiological internal solution in the electrode, which leads to calcium influx and potassium efflux from LCs (*10*). This type of LC activation also led to robust AP firing (Fig. 4, D, E, and G, and fig. S7, C and D). The onset of afferent firing was variable, commencing 87 to 288 ms after the start of current injections and 20 to 9120 ms after the start of depolarizations, with an apparent trend toward reduced number of APs toward the end of the stimulus (Fig. 4F). Thus, activation of a single LC is sufficient to drive AP firing in the afferent, demonstrating that LCs can transmit touch information to the afferent.

Next, we sought to probe the mechanism of LC-afferent communication. Because mechanical stimulation of LCs leads to AP firing via voltage-gated calcium channels (*10*), we hypothesized that such a mechanism could depend on calcium entry into LC. Depolarization of LCs activates both voltage-activated calcium and voltage-activated potassium channels. First, we quenched potassium efflux by including cesium chloride in the intracellular solution. Under these conditions, activation of LCs successfully induced AP firing in the afferent (Fig. 5A). However, the removal of calcium from the extracellular medium and simultaneous blockade of voltage-gated calcium channels by cadmium suppressed LC-induced firing in the afferent, and the effect was reversed upon reintroduction of the original extracellular medium (Fig. 5, A and B). These data demonstrate that calcium influx during LC activation is an essential prerequisite for LC-afferent communication.

DISCUSSION

Together with earlier observations that avian Meissner LCs are mechanosensitive and excitable (*10*), these results establish LCs as physiological sensors of touch. Activation of LCs did not result in immediate excitability changes in the afferent, but instead induced irregular firing with variable delays, arguing against direct electrical coupling. This is consistent with the earlier finding that LCs lack functional gap junctions with surrounding cells (*10*). The presence of exocytotic machinery in LCs instead suggests that communication with afferent fibers may involve chemical transmission (*15*, *16*). In support of this idea, the removal of extracellular calcium abolished LC-induced firing in the afferent, suggesting a possible involvement of calcium-dependent vesicular communication. Other mechanisms, including ephaptic cross-talk, may also be used. Tethers connecting the membranes of LCs and afferents could provide another alternative, mediating mechanical coupling between cellular elements and/or gating of mechanically activated ion channels (*17*–*19*). These tethers may also have important biomechanical consequences for the transduction of touch within the corpuscle.

Our findings provide support for a model of touch detection in Meissner corpuscles by the afferent and LCs. The physiological consequences of a bicellular mechanism to detect touch are intriguing. Although mechanoreceptive afferents faithfully fired APs during dynamic stimulation of corpuscles, LCs induced afferent firing with latencies ranging from 20 ms to up to ~9 s. Thus, LCs are

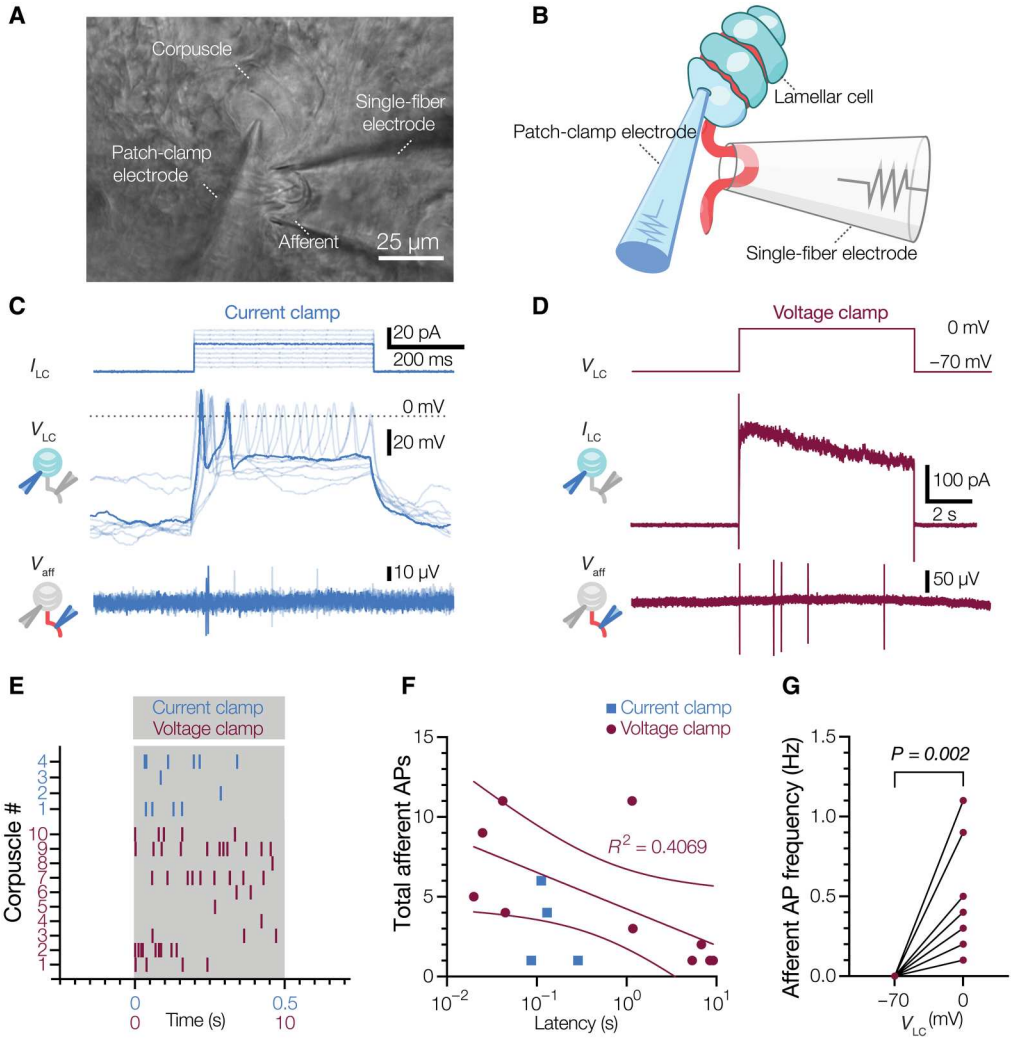

Fig. 4. Activation of a single LC is sufficient to drive afferent firing. (**A** and **B**) Bright-field image (A) and schematic representation of the experimental setup (B) for simultaneous electrophysiological recordings from LC and afferent of a Meissner corpuscle in duck bill skin. (**C**) Current injection applied to the LC (I_{LC}, top), voltage response and APs in the LC recorded with a potassium-based internal solution (V_{LC}, middle), and extracellular voltage and APs in the afferent (V_{aff}, bottom). (**D**) Voltage step stimulus applied to the LC (V_{LC}, top), current response with potassium-based internal solution in the LC (I_{LC}, middle), and extracellular voltage and APs in the afferent (V_{aff}, bottom). (**E**) Raster plot of afferent AP firing for individual corpuscles during LC activation by either depolarizing current injections in the current clamp (blue) or voltage steps to 0 mV in the voltage clamp (maroon). Each vertical dash represents an individual AP. (**F**) Total number of afferent APs versus latency between onset of the stimulus and first AP. Dots represent data from individual corpuscles. The solid line is a fit to the liner equation and dashed lines are 95% confidence intervals of the linear fit. (**G**) Afferent AP frequency when LCs held at −70 and 0 mV. Lines connect data pairs from individual corpuscles. Wilcoxon matched pairs test.

likely not responsible for the fast primary mechanosensory response observed in the afferent (*12*). Rather, it is expected that sensory afferents directly mediate this response via Piezo2 (*4*, *20*, *21*) and that LCs perform a yet unidentified but complementary role in touch detection. Such a bicellular mechanism, which includes the afferents and LCs, would enable multifaceted mechanosensation, potentially facilitating more versatile and precise detection of touch.

Ducks present an attractive model to inquire into general principles of mechanoreceptor function in vertebrates from the perspective of a tactile specialist animal. Duck bill skin contains a high-density population of Meissner (Grandry) and Pacinian (Herbst) corpuscles accessible to electrophysiological and structural studies (*3*, *9*, *12*, *22*–*24*). Avian Meissner corpuscles are structurally and functionally similar to their mammalian counterparts. Meissner corpuscles endow humans with the remarkable ability to manipulate objects and tools, facilitate sensorimotor control in mice, and enable tactile specialist birds to carry out a multitude of foraging behaviors (*2*, *8*, *25*–*27*). While this manuscript was finalized, a preprint study reported the 3D architecture of the mouse Meissner corpuscle by FIB-SEM, which, together with earlier literature, permits a detailed comparison with the avian structure (*28*). Both corpuscles contain a stack of LCs innervated by one or two afferents which are mostly, though not exclusively, rapidly adapting. At the same time, some differences exist between the two. Unlike mammalian corpuscles, avian LCs do not form extensive lamellae, and the afferent terminals in avian LCs have a limited number of protrusions compared to mammalian counterparts. In addition, numerous DCVs are present in avian LCs but have not been reported in mammalian

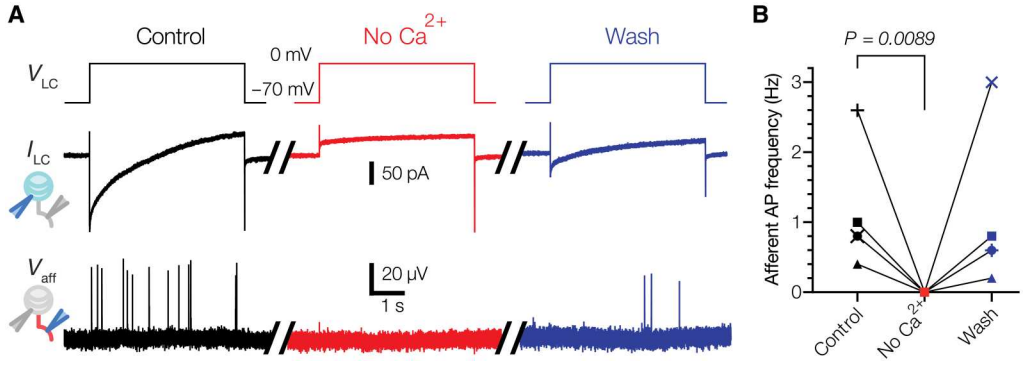

Fig. 5. LC activation triggers afferent firing via a calcium-dependent mechanism. (**A**) Exemplar traces recorded in a Meissner afferent in response to LC activation by voltage clamp with a cesium-based internal solution to quench potassium efflux (control), following the removal of extracellular Ca^{2+} and the addition of 300 μM Cd^{2+} to block voltage-activated calcium channels (No Ca^{2+}) and upon reintroduction of calcium and removal of Cd^{2+} (Wash). V_{LC}, voltage step stimulus applied to the LC; I_{LC}, current response in the LC; V_{aff}, extracellular voltage and APs in the afferent. (**B**) Quantification of the effect of calcium removal on LC-induced afferent firing. Lines connect data from the same afferent ($n = 5$ afferents). The difference between control and wash was not significant ($P = 0.6856$). Friedman test with Dunn's correction for multiple comparisons.

Meissner LCs (*8*, *28*). Despite these differences, avian and mammalian corpuscles detect the same stimuli—transient touch and low-frequency vibration—and transmit sensory information via AP firing during the dynamic phase of the stimulus (*2*, *8*, *9*, *12*–*14*, *19*, *22*, *28*). Although additional research is needed to evaluate the role of the different structural components, current data suggest that the mechanism of corpuscle function may rely on the interplay between LCs and the afferent terminal via chemical communication and possibly physical interactions via tethers. A unifying theme found in avian and mammalian corpuscles is the close association and large contact area between LCs and afferent terminals. The remarkable functional and structural homogeneity between avian and mammalian Meissner corpuscles suggests that the physiological role of LCs is conserved between species. Whether LCs from mammalian corpuscles are mechanosensitive remains to be determined but appears likely given that dissociated murine Schwann cells are mechanosensitive in culture, and inhibition of these cells via optogenetics increases the threshold of touch detection transmitted by Meissner afferent (*6*, *7*). LCs from both avian and mammalian Meissner corpuscles are of mesenchymal origin, similar to the inner core cells in Pacinian corpuscles but dissimilar to epidermal Merkel cells (*29*–*32*). This suggests that other vertebrate end organs in which TSCs are in close association with afferent fibers, including Pacinian corpuscles and hair follicles, may use them to detect tactile stimuli (*3*).

MATERIALS AND METHODS

Animals

Experiments with Mallard duck embryos (*Anas platyrhynchos domesticus*) were approved by and performed in accordance with the guidelines of the Institutional Animal Care and Use Committee of Yale University (protocol 11526). Animals used in experiments were at developmental stages embryonic day 25 (E25) to E27 unless otherwise indicated; sex was not determined.

Ex vivo bill skin preparation

Dissection of bill skin was performed as described previously (*12*). Briefly, the glabrous skin of the bill was quickly cut from the embryo in ice-cold L-15 media. The bill skin was placed with the dermis on top and epidermis on the bottom in a recording chamber in Krebs solution containing (in millimolar) 117 NaCl, 3.5 KCl, 2.5 $CaCl_2$, 1.2 $MgCl_2$, 1.2 NaH_2PO_4, 25 $NaHCO_3$, and 11 glucose, saturated with 95% O_2 and 5% CO_2 (pH 7.3 to 7.4), at room temperature (22° to 23°C). Corpuscles in the dermis were visualized on an Olympus BX51WI upright microscope with an ORCA-Flash 4.0 LT camera (Hamamatsu). The bill skin was treated with collagenase P (2 mg/ml; Roche) in Krebs solution for 5 min, and then washed with fresh Krebs solution before recording.

Electrophysiology

Single-fiber recording

Recordings from single afferent fibers of avian Meissner (Grandry) corpuscles were acquired at room temperature in Krebs solution using a MultiClamp 700B amplifier and Digidata 1550A digitizer (Molecular Devices). Single-fiber recording pipettes were created from thin-walled, 1.5-mm-diameter borosilicate glass capillaries. Pipettes were pulled using a P-1000 micropipette puller (Sutter Instruments) to create tip diameters of 5 to 30 μm, and then filled with Krebs solution. Pipettes were placed on a CV-7B headstage connected to a High Speed Pressure Clamp (ALA Scientific Instruments). Single corpuscles and connected afferents within the same field of view were identified under a 40× objective lens. The recording pipette was placed next to the afferent, and negative pressure was applied until a large section (~5 μm) of the afferent was sucked into the pipette. The extracellular afferent voltage was recorded in the current clamp mode, sampled at 20 kHz and low-pass filtered at 1 kHz. A suprathreshold mechanical step or 20-Hz vibrating stimulus was applied to the connected corpuscle to confirm the presence of mechanically induced APs in the afferent fiber. Fresh Krebs solution was regularly perfused onto the preparation between recordings.

Mechanical stimuli were applied to a single corpuscle using a blunt glass probe (5- to 10-μm tip diameter) mounted on a piezoelectric-driven actuator (Physik Instrumente Gmbh). A mechanical step stimulus was applied to corpuscles with variable displacements in increments of 1 μm. The duration of the static phase of the step stimulus was constant at 150 ms. The duration of the dynamic

phases of the step stimulus was 3 or 30 ms to record single or multiple APs within the displacement ramp, respectively. Vibratory stimuli were applied using a 20-Hz sinusoidal waveform with a constant amplitude between 1 and 38 μm.

Patch-clamp electrophysiology

Recordings of LCs were performed as described previously (*10*) with simultaneous single-fiber recording in the Krebs solution described above. Standard-wall, 1.5-mm-diameter borosilicate pipettes with tip resistances of 2 to 4 megohms were used to acquire LC voltage clamp and current clamp recordings. Pipettes were filled with (in millimolar) 135 K-gluconate, 5 KCl, 0.5 $CaCl_2$, 2 $MgCl_2$, 5 EGTA, 5 Hepes, 5 Na_2ATP, and 0.5 Na_2GTP (pH 7.3 with KOH) and placed on a secondary CV-7B headstage (connected to a second High Speed Pressure Clamp) which was placed perpendicular to the primary headstage. After single-fiber recordings were established for an individual corpuscle, the whole-cell recording configuration was achieved for one of the LCs within the corpuscle. LC current and voltage data were sampled at 20 kHz and low-pass filtered at 2 kHz.

LCs were activated by current injection in a current clamp or a voltage step in a voltage clamp, while the afferent activity was measured simultaneously via single-fiber recording. In the current clamp, depolarizing current steps (from 10 to 120 pA in 10-pA increments) were applied to elicit voltage-gated calcium channel-mediated APs in the LC. In a voltage clamp, the LC was initially held at −70 mV, and then clamped at 0 mV for 10 s. Mechanical step stimuli were applied before and after LC activation protocols to elicit mechanoreceptor APs, confirming the health and proper function of the corpuscle and afferent throughout the experiment. To test the potential mechanism of LC-afferent communication, LCs were held at −70 mV, and then voltage-clamped at 0 mV for 5 s while measuring afferent activity in each experimental condition. An intracellular solution containing (in millimolar) 133 CsCl, 10 Hepes, 5 EGTA, 1 $CaCl_2$, 1 $MgCl_2$, 4 MgATP, and 0.4 Na_2GTP (pH 7.3 with CsOH) was used in LCs to block potassium current. To block calcium influx, Krebs solution containing 20 μM $CaCl_2$ and 300 μM $CdCl_2$ was added, and then washed off with normal Krebs solution.

Single-fiber and patch-clamp recordings were acquired from individual corpuscles in skin preparations from different animals. Electrophysiological data were obtained in Clampfit 10.7 (Molecular Devices), and then analyzed and displayed in GraphPad Prism 9.5.1 (GraphPad Software, LLC).

FIB-SEM

EM sample preparation

The immersion fixation protocol was adapted from the mouse skin preparation method (*8*). A patch of bill skin was dissected from a duck embryo and immediately immersed in a fixative solution containing 2.5% glutaraldehyde, 2.5% paraformaldehyde, 0.13 M cacodylate, 4 mM CaCl2, and 4 mM MgCl2 (pH 7.4, 37°C). The epidermis was removed while the skin patch remained in this solution, and the skin was cut into 1 mm by 1 mm sections at room temperature. After 2 hours, the dermis was transferred to a fresh solution and gently shaken at 4°C for 48 hours. The solution was replaced with a freshly prepared fixative at the 24-hour time point. After 48 hours, the sample was stored in a solution of 1.5% paraformaldehyde and 0.13 M cacodylate (pH 7.4) and stored at 4°C.

The bill skin samples were then sectioned into 300-μm-thick slices in 0.13 M cacodylate buffer using a Compresstome (Precisionary, MA). The slices were washed in cacodylate buffer (0.13 M), postfixed with 2% osmium tetroxide, and 1.5% potassium ferrocyanide in 0.13 M cacodylate buffer for 120 min at 0°C. After washing in distilled water, the slices were stained with 1% thiocarbohydrazide for 40 min at 40°C and 2% osmium tetroxide for 90 min at room temperature followed by 1% uranyl acetate at 4°C overnight. These staining reagents were diluted in double distilled water. The sample slices were completely washed with distilled water between each step at room temperature three times for 10 min each. Last, the slices were transferred into lead aspartate solution at 50°C for 120 min followed by distilled water wash at room temperature three times for 10 min each. After the heavy metal staining procedure, the samples were dehydrated with graded ethanol, embedded in Durcupan resin (Sigma-Aldrich, MO), and then polymerized at 60°C for 48 hours.

FIB-SEM sample preparation

One Durcupan-embedded duck bill skin sample contained one whole Meissner corpuscle and one partial Meissner corpuscle (DB.B2-01M), and another sample contained one whole Meissner and one whole Pacinian corpuscle (DB.B2-01MP). The sample was first mounted to the top of a 1-mm copper post which was in contact with the metal-stained sample for better charge dissipation, as previously described (*33*). The vertical sample post was trimmed to a small block containing one Meissner corpuscle with the width perpendicular to the ion beam, and the depth in the direction of the ion beam sequentially (*34*). The block size was 110 × 80 μm^2. After the entire volume of DB.B2-01M was FIB-SEM–imaged, the sample post was then trimmed to sample DB.B2-01MP that contains a region of interest (ROI) of one Meissner conjunction with one Pacinian corpuscle (DB.B2-01MP) with a block size of 135 × 110 μm^2. The trimming was guided by x-ray tomography data obtained by a Zeiss Versa XRM-510 and optical inspection under a microtome. Thin layers of conductive material of 10-nm gold followed by 100-nm carbon were coated on the trimmed samples using a Gatan 682 High-Resolution Ion Beam Coater. The coating parameters were 6 keV, 200 nA on both argon gas plasma sources, and 10 rpm sample rotation with 45° tilt.

FIB-SEM 3D large volume imaging

Two FIB-SEM prepared samples, DB.B2-01M and DB.B2-01MP, were imaged sequentially by two customized Zeiss FIB-SEM systems previously described (*33*, *35*, *36*). The block face of ROI was imaged by a 2-nA electron beam with 1.2-keV landing energy at a 2-MHz scanning rate. The *x*-*y* pixel resolution was set at 8 nm. A subsequently applied focused Ga^+ beam of 15 nA at 30 keV strafed across the top surface and ablated away 8 nm of the surface. The newly exposed surface was then imaged again. The ablation imaging cycle continued about once every half minute for 4 days to complete FIB-SEM imaging DB.B2-01M which contains one Meissner corpuscle and about once every minute for 1 week to complete DB.B2-01MP that contains one Meissner corpuscle and one Pacinian corpuscle. The acquired image stack formed a raw imaged volume, followed by postprocessing of image registration and alignment using a Scale Invariant Feature Transform–based algorithm. The aligned stack consists of a final isotropic volume of 60 × 50 × 58 μm^3 and 85 × 56 × 75 μm^3 for DB.B2-01M and DB.B2-01MP, respectively. The voxel size of 8 × 8 × 8 nm^3 was maintained

for both samples throughout entire volumes, which can be viewed in any arbitrary orientation.

FIB-SEM segmentation

The segmentations of organelles, cells, and nuclei from FIB-SEM images were achieved with Apeer, an AI-driven cloud-based platform (www.apeer.com/) (*37*). Deep learning techniques were used to achieve automated segmentation, using a customized convolutional neural network (CNN) architecture based on 2D U-Net. To generate ground truth data, cells and organelles were manually annotated from a small set (100 planes) of the raw FIB-SEM images. The CNNs were trained using the annotated ground truth data and proofread to achieve high-quality segmentation of the objects in 3D. Semantic segmentation was applied to each object, and the accuracy of the segmentation was assessed by evaluating the voxel Intersection over Union (IoU) and F1 scores. IoU was calculated as the overlap between annotation and ground truth bounding boxes by computing the ratio of the intersection area to the union area: IoU = (Intersection Area)/(Union Area). The F1 score was calculated as the balance between the model's ability to correctly identify positive samples (precision) and its ability to capture all positive samples (recall): F1 = 2 * (Precision * Recall)/(Precision + Recall) (*38*). Apeer machine learning models were downloaded separately for each class of cells or organelles to create a full 3D model on a full dataset. All volumes were segmented at 16 × 16 × 16 nm resolution except DCVs which were segmented at 8 × 8 × 8 nm.

FIB-SEM reconstruction and data analysis

Raw FIB-SEM data and Apeer machine learning models for each class were imported into Arivis Vision 4D software. Using this software, each individual cell and organelle was segmented to generate complete objects, which were then filtered by size to remove any extraneous noise components. The objects were manually proofread and adjusted as necessary, and various quantitative measures such as volume, distances, surface area, and diameters were calculated within the software. The diameter of each DCV was estimated by identifying the longest and shortest path between two mesh nodes. The contact area between the LC and the afferent was determined by dilating each object by 1 pixel, creating their intersection, and dividing the resulting surface area by two. Python scripts were used to calculate density scores for the DCVs, and videos were generated using Arivis Vision 4D. Three-dimensional tomography was reconstructed at 1.6 × 1.6 × 1.6 nm resolution manually per plane using Arivis Vision 4D software.

Reconstructed model in 3D: https://sketchfab.com/3d-models/avian-meissner-grandry-corpuscle-4175eadcd2aa4005b4bbbc2e163ead35

3D transmission electron microscopy tomography

Freshly peeled duck bill skin was fixed in Karnovsky fixative at 4°C for 1 hour, washed in 0.1 M sodium cacodylate buffer (pH 7.4), and then postfixed in 1% osmium tetroxide for 1 hour in the dark on ice. The tissue was stained in Kellenberger solution for 1 hour at room temperature after washing in distilled water, dehydrated in a series of alcohols and propylene oxide, then embedded in EMbed 812, and polymerized overnight at 60°C. Thick sections of 250-nm depth were obtained from hardened blocks using a Leica UltraCut UC7 on copper formvar–coated slot grids. Sections (250-nm thick) were contrast stained using 2% uranyl acetate and lead citrate, and 15-nm fiducial gold was added to both sides to aid alignment for tomography. Sections were viewed using a FEI Tecnai TF20 at 200 Kv and data were collected using SerialEM (*39*) on a FEI Eagle 4Kx4K charge-coupled device camera using tilt angles of −60° to 60°, and then reconstructed in IMOD (University of Colorado, Boulder). All solutions were supplied by Electron Microscopy Sciences (Hatfield, PA).

RNA sequencing of individual corpuscles

Corpuscles were manually collected and pooled for subsequent transcriptomic analysis in ribonuclease-free conditions. Aspiration pipettes pulled from capillary glass tubing (G150F-3, Warner Instruments, Hamden, CT) using a micropipette puller (P-1000, Sutter, Novato, CA) had a tip diameter of ~40 to 60 μM and were filled with 3 μl of the RNA lysis buffer (Quick-RNA Microprep Kit, Zymo, Irvine, Ca). The pipette was mounted on a micromanipulator and used to aspirate 2 to 10 corpuscles from duck bill skin by applying negative pressure using a High Speed Pressure Clamp system (HSPC-1, ALA Scientific Instruments). Collected corpuscles were deposited into a 0.5-ml tube containing 10 μl of the RNA lysis buffer. Nearby skin cells devoid of any corpuscles were collected for comparison. Samples were then stored at −80°C until RNA isolation. Five to six total replicates were collected from three independent skin isolations. RNA was isolated using the Quick-RNA Microprep Kit (Zymo) according to the manufacturer's instructions. RNA concentration and integrity number (RIN) were assessed by Agilent 2100 Bioanalyzer (Agilent, Santa Clara, CA). RNA concentrations for corpuscles were in the range of 63 to 323 pg/μl and RIN values were in the range of 6.1 to 8.0.

Library preparation and sequencing were carried out at the Yale Center for Genome Analysis. Sequencing libraries were prepared using the Kapa mRNA Hyper Prep kit (KAPA Biosystems, Wilmington, MA) (skin samples) or the NEBNext Single Cell/Low Input RNA Library Prep Kit (New England Biolabs, Ipswich, MA) (corpuscle samples). Libraries were sequenced on the Illumina NovaSeq instrument in the 150–base pair paired-end mode according to the manufacturer's protocols. A total of ~30 million to 52 million sequencing read pairs per sample were obtained.

The sequencing data were processed on the Yale Center for Research Computing cluster. Raw sequencing reads were filtered and trimmed to retain high-quality reads using Trimmomatic v0.39 (*40*) with default parameters. Filtered high-quality reads from all samples were aligned to the duck reference genome using the STAR aligner v2.7.7a with default parameters (*41*). Statistical analysis of differential expression of genes between groups was performed using the generalized linear model (GLM) approach and the quasi-likelihood *F* test, as implemented in the EdgeR package. The duck reference genome and the gene annotation were obtained from the National Center for Biotechnology Information (*Anas platyrhynchos*; assembly ZJU1.0; NCBI Annotation Release: 104; all files accessed on 4/30/2021).

Reference genome: https://ftp.ncbi.nlm.nih.gov/genomes/all/GCF/015/476/345/GCF_015476345.1_ZJU1.0/GCF_015476345.1_ZJU1.0_genomic.fna.gz.

Gene annotation: https://ftp.ncbi.nlm.nih.gov/genomes/all/GCF/015/476/345/GCF_015476345.1_ZJU1.0/GCF_015476345.1_ZJU1.0_genomic.gff.gz.

The gene annotation was filtered to include only protein-coding genes. Aligned reads were counted by the featureCounts module within the Subread package v2.0.1 using the "unstranded" mode with default parameters (*42*). Read counting was performed at the

gene level, i.e., the final read count for each gene included all reads mapped to all exons of the gene. Processing, normalization, and statistical analysis of read counts were performed using the EdgeR v3.38.4 package in R v4.2.1 (*43*). Normalized read counts were obtained by normalizing raw read counts to the effective library sizes of each sample. Effective library sizes were calculated by normalizing raw library sizes by RNA composition using a trimmed mean of *M* values method, as implemented in the calcNormFactors function of the EdgeR package. Normalized read counts were further normalized to gene length and expressed as "fragments per kilobase gene length per million mapped reads". Statistical analysis of differential expression of genes between groups was performed using the GLM approach and the quasi-likelihood *F* test, as implemented in the EdgeR package. RNA sequencing data were deposited to the Gene Expression Omnibus (accession number GSE218686).

Supplementary Materials

This PDF file includes:
Figs. S1 to S7
Table S1
Legends for movies S1 to S5

Other Supplementary Material for this manuscript includes the following:
Movies S1 to S5

REFERENCES AND NOTES

1. L. L. Orefice, A. L. Zimmerman, A. M. Chirila, S. J. Sleboda, J. P. Head, D. D. Ginty, Peripheral mechanosensory neuron dysfunction underlies tactile and behavioral deficits in mouse models of ASDs. *Cell* **166**, 299–313 (2016).
2. A. Handler, D. D. Ginty, The mechanosensory neurons of touch and their mechanisms of activation. *Nat. Rev. Neurosci.* **22**, 521–537 (2021).
3. E. R. Schneider, E. O. Gracheva, S. N. Bagriantsev, evolutionary specialization of tactile perception in vertebrates. *Phys. Ther.* **31**, 193–200 (2016).
4. S. S. Ranade, S. H. Woo, A. E. Dubin, R. A. Moshourab, C. Wetzel, M. Petrus, J. Mathur, V. Bégay, B. Coste, J. Mainquist, A. J. Wilson, A. G. Francisco, K. Reddy, Z. Qiu, J. N. Wood, G. R. Lewin, A. Patapoutian, Piezo2 is the major transducer of mechanical forces for touch sensation in mice. *Nature* **516**, 121–125 (2014).
5. J. M. Kefauver, A. B. Ward, A. Patapoutian, Discoveries in structure and physiology of mechanically activated ion channels. *Nature* **587**, 567–576 (2020).
6. H. Abdo, L. Calvo-Enrique, J. M. Lopez, J. Song, M. D. Zhang, D. Usoskin, A. el Manira, I. Adameyko, J. Hjerling-Leffler, P. Ernfors, Specialized cutaneous Schwann cells initiate pain sensation. *Science* **365**, 695–699 (2019).
7. J. Ojeda-Alonso, L. Calvo-Enrique, R. Paricio-Montesinos, R. Kumar, M.-D. Zhang, J. F. A. Poulet, P. Ernfors, G. R. Lewin. Sensory Schwann cells set perceptual thresholds for touch and selectively regulate mechanical nociception. bioRxiv 2022.2002.2004.477749 (2023). https://doi.org/10.1101/2022.02.04.477749.
8. N. L. Neubarth, A. J. Emanuel, Y. Liu, M. W. Springel, A. Handler, Q. Zhang, B. P. Lehnert, C. Guo, L. L. Orefice, A. Abdelaziz, M. M. DeLisle, M. Iskols, J. Rhyins, S. J. Kim, S. J. Cattel, W. Regehr, C. D. Harvey, J. Drugowitsch, D. D. Ginty, Meissner corpuscles and their spatially intermingled afferents underlie gentle touch perception. *Science* **368**, eabb2751 (2020).
9. L. H. Ziolkowski, E. O. Gracheva, S. N. Bagriantsev, Tactile sensation in birds: Physiological insights from avian mechanoreceptors. *Curr. Opin. Neurobiol.* **74**, 102548 (2022).
10. Y. A. Nikolaev, V. V. Feketa, E. O. Anderson, E. R. Schneider, E. O. Gracheva, S. N. Bagriantsev, Lamellar cells in Pacinian and Meissner corpuscles are touch sensors. *Sci. Adv.* **6**, eabe6393 (2020).
11. R. Cobo. *Somatosensory and Motor Research* (IntechOpen, 2020), pp. 1–15.
12. L. H. Ziolkowski, E. O. Gracheva, S. N. Bagriantsev, Mechanotransduction events at the physiological site of touch detection. *eLife* **12**, e84179 (2023).
13. K. M. Gottschaldt, The physiological basis of tactile sensibility in the beak of geese. *J. Comp. Physiol.* **95**, 29–47 (1974).
14. K. M. Gottschaldt, S. Lausmann, Mechanoreceptors and their properties in the beak skin of geese (Anser anser). *Brain Res.* **65**, 510–515 (1974).
15. W. Chang, H. Kanda, R. Ikeda, J. Ling, J. DeBerry, J. G. Gu, Merkel disc is a serotonergic synapse in the epidermis for transmitting tactile signals in mammals. *Proc. Natl. Acad. Sci. U.S.A.* **113**, E5491–E5500 (2016).
16. B. U. Hoffman, Y. Baba, T. N. Griffith, E. V. Mosharov, S. H. Woo, D. D. Roybal, G. Karsenty, A. Patapoutian, D. Sulzer, E. A. Lumpkin, Merkel cells activate sensory neural pathways through adrenergic synapses. *Neuron* **100**, 1401–1413.e6 (2018).
17. J. Hu, L. Y. Chiang, M. Koch, G. R. Lewin, Evidence for a protein tether involved in somatic touch. *EMBO J.* **29**, 855–867 (2010).
18. L. Li, D. D. Ginty, The structure and organization of lanceolate mechanosensory complexes at mouse hair follicles. *eLife* **3**, e01901 (2014).
19. F. Schwaller, V. Bégay, G. García-García, F. J. Taberner, R. Moshourab, B. McDonald, T. Docter, J. Kühnemund, J. Ojeda-Alonso, R. Paricio-Montesinos, S. G. Lechner, J. F. A. Poulet, J. M. Millan, G. R. Lewin, USH2A is a Meissner's corpuscle protein necessary for normal vibration sensing in mice and humans. *Nat. Neurosci.* **24**, 74–81 (2021).
20. Y. Garcia-Mesa, J. Feito, P. Cuendias, J. García-Piqueras, A. Germanà, O. García-Suárez, B. Martín-Biedma, J. A. Vega, The acquisition of mechanoreceptive competence by human digital Merkel cells and sensory corpuscles during development: An immunohistochemical study of PIEZO2. *Ann Anat* **243**, 151953 (2022).
21. Y. Garcia-Mesa, J. García-Piqueras, B. García, J. Feito, R. Cabo, J. Cobo, J. A. Vega, O. García-Suárez, Merkel cells and Meissner's corpuscles in human digital skin display Piezo2 immunoreactivity. *J. Anat.* **231**, 978–989 (2017).
22. E. R. Schneider, E. O. Anderson, M. Mastrotto, J. D. Matson, V. P. Schulz, P. G. Gallagher, R. H. LaMotte, E. O. Gracheva, S. N. Bagriantsev, Molecular basis of tactile specialization in the duck bill. *Proc. Natl. Acad. Sci. U.S.A.* **114**, 13036–13041 (2017).
23. E. R. Schneider, E. O. Anderson, V. V. Feketa, M. Mastrotto, Y. A. Nikolaev, E. O. Gracheva, S. N. Bagriantsev, A cross-species analysis reveals a general role for Piezo2 in mechanosensory specialization of trigeminal ganglia from tactile specialist birds. *Cell Rep.* **26**, 1979–1987.e3 (2019).
24. E. R. Schneider, M. Mastrotto, W. J. Laursen, V. P. Schulz, J. B. Goodman, O. H. Funk, P. G. Gallagher, E. O. Gracheva, S. N. Bagriantsev, Neuronal mechanism for acute mechanosensitivity in tactile-foraging waterfowl. *Proc. Natl. Acad. Sci. U.S.A.* **111**, 14941–14946 (2014).
25. H. Berkhoudt, The morphology and distribution of cutaneous mechanoreceptors (Herbst and Grandry corpuscles) in bill and tongue of the Mallard (*Anas platyrhynchos* L.). *Neth J. Zool.* **30**, 1–34 (1980).
26. A. K. West, E. M. Xu, M. D. Nelson, T. R. Hart, E. M. Stricker, A. G. Cones, G. M. Martin, K. Strickland, D. L. Lambert, L. Burman, B. H. Zhu, E. R. Schneider, quantitative evaluation of tactile foraging behavior in Pekin and Muscovy ducks. *Front. Physiol.* **13**, 921657 (2022).
27. G. A. Zweers, Mechanics of the feeding of the mallard (*Anas platyrhynchos* L.; Aves, Anseriformes), in *Contributions to Vertebrate Evolution* (S Karger Pub, ed. 1, 1977).
28. A. Handler, Q. Zhang, S. Pang, T. M. Nguyen, M. Iskols, M. Nolan-Tamariz, S. Cattel, R. Plumb, B. Sanchez, K. Ashjian, A. Shotland, B. Brown, M. Kabeer, J. Turecek, G. Rankin, W. Xiang, E. C. Pavarino, N. Africawala, C. Santiago, W-C. A. Lee, C. S. Xu, D. D. Ginty. Three-dimensional reconstructions of mechanosensory end organs suggest a unifying mechanism underlying dynamic, light touch. bioRxiv 2023.2003.2017.533188 (2023). https://doi.org/10.1101/2023.03.17.533188.
29. C. Ide, B. L. Munger, A cytologic study of Grandry corpuscle development in chicken toe skin. *J. Comp. Neurol.* **179**, 301–324 (1978).
30. R. Ikeda, M. Cha, J. Ling, Z. Jia, D. Coyle, J. G. Gu, Merkel cells transduce and encode tactile stimuli to drive Aβ-Afferent impulses. *Cell* **157**, 664–675 (2014).
31. S. Maksimovic, M. Nakatani, Y. Baba, A. M. Nelson, K. L. Marshall, S. A. Wellnitz, P. Firozi, S. H. Woo, S. Ranade, A. Patapoutian, E. A. Lumpkin, Epidermal Merkel cells are mechanosensory cells that tune mammalian touch receptors. *Nature* **509**, 617–621 (2014).
32. S. H. Woo, S. Ranade, A. D. Weyer, A. E. Dubin, Y. Baba, Z. Qiu, M. Petrus, T. Miyamoto, K. Reddy, E. A. Lumpkin, C. L. Stucky, A. Patapoutian, Piezo2 is required for Merkel-cell mechanotransduction. *Nature* **509**, 622–626 (2014).
33. C. S. Xu, K. J. Hayworth, Z. Lu, P. Grob, A. M. Hassan, J. G. García-Cerdán, K. K. Niyogi, E. Nogales, R. J. Weinberg, H. F. Hess, Enhanced FIB-SEM systems for large-volume 3D imaging. *eLife* **6**, (2017).
34. S. Pang, C. S. Xu, Methods of enhanced FIB-SEM sample preparation and image acquisition. *Methods Cell Biol.* **177**, 269–300 (2023).
35. C. S. Xu, S. Pang, G. Shtengel, A. Müller, A. T. Ritter, H. K. Hoffman, S. Y. Takemura, Z. Lu, H. A. Pasolli, N. Iyer, J. Chung, D. Bennett, A. V. Weigel, M. Freeman, S. B. van Engelenburg, T. C. Walther, R. V. Farese Jr., J. Lippincott-Schwartz, I. Mellman, M. Solimena, H. F. Hess, An open-access volume electron microscopy atlas of whole cells and tissues. *Nature* **599**, 147–151 (2021).
36. C. S. Xu, K. J. Hayworth, H. F. Hess, Enhanced FIB-SEM systems for large-volume 3D imaging. U.S. patent no. 10,600,615 B2 (2020).

37. D. Dang. *APEER: An Interactive Cloud Platform for Microscopists to Easily Deploy Deep Learning* (Zenodo, 2021); https://zenodo.org/record/5539895.
38. R. Padilla, S. L. Netto, E. A. B. d. Silva, *2020 International Conference on Systems, Signals and Image Processing (IWSSIP)*, Niteroi, Rio de Janeiro, Brazil, 1 to 3 July 1-3, 2020 (2020), pp. 237–242.
39. D. N. Mastronarde, Automated electron microscope tomography using robust prediction of specimen movements. *J. Struct. Biol.* **152**, 36–51 (2005).
40. A. M. Bolger, M. Lohse, B. Usadel, Trimmomatic: A flexible trimmer for Illumina sequence data. *Bioinformatics* **30**, 2114–2120 (2014).
41. A. Dobin, C. A. Davis, F. Schlesinger, J. Drenkow, C. Zaleski, S. Jha, P. Batut, M. Chaisson, T. R. Gingeras, STAR: Ultrafast universal RNA-seq aligner. *Bioinformatics* **29**, 15–21 (2013).
42. Y. Liao, G. K. Smyth, W. Shi, featureCounts: An efficient general purpose program for assigning sequence reads to genomic features. *Bioinformatics* **30**, 923–930 (2014).
43. M. D. Robinson, D. J. McCarthy, G. K. Smyth, edgeR: A Bioconductor package for differential expression analysis of digital gene expression data. *Bioinformatics* **26**, 139–140 (2010).

Acknowledgments: We thank members of the Bagriantsev and Gracheva laboratories for comments and critique throughout the study; M. Graham, X. Liu, and Yale School of Medicine Electron Microscopy Core for transmission electron microscopic imaging for electron tomography; D. Ginty for sharing the skin sample fixation protocol; S. A. Mentone for help with skin tissue fixation; G. Parlakgül, A. Bergen, and M. Burdyniuk for advice on FIB-SEM data processing; B. Bae and S. Bae for help with electron microscopy image processing for 3D reconstruction. **Funding:** This work was funded by a Gruber Foundation Fellowship (to L.H.Z.), Howard Hughes Medical Institute (to S.P., W.-P.L., and C.S.X.), National Science Foundation grants 1754286 (to E.O.G.) and 1923127 (to S.N.B.), and NIH grants R01NS097547 and R01NS126277 (to S.N.B.). **Author contributions:** Conceptualization: Y.A.N., L.H.Z., E.O.G., and S.N.B. Data collection: Y.A.N., L.H.Z., S.P., W.-P.L., V.V.F., and C.S.X. Funding acquisition, project administration, and supervision: C.S.X., E.O.G., and S.N.B. Writing: Y.A.N., L.H.Z., E.O.G., and S.N.B. **Competing interests:** C.S.X. is an inventor of a U.S. patent assigned to Howard Hughes Medical Institute for the enhanced FIB-SEM systems used in this work: C.S.X., K. J. Hayworth, and H. F. Hess (2020) "Enhanced FIB-SEM systems for large-volume 3D imaging." U.S. patent no. 10,600,615, 24 Mar 2020. The other authors declare that they have no competing interests. **Data and materials availability:** All data needed to evaluate the conclusions in the paper are present in the paper and/or the Supplementary Materials. RNA sequencing data are deposited to the Gene Expression Omnibus (accession number GSE218686).

Submitted 24 April 2023
Accepted 9 August 2023
Published 13 September 2023
10.1126/sciadv.adi4147

ScienceAdvances

3D architecture and a bicellular mechanism of touch detection in mechanosensory corpuscle

Yury A. Nikolaev, Luke H. Ziolkowski, Song Pang, Wei-Ping Li, Viktor V. Feketa, C. Shan Xu, Elena O. Gracheva, and Sviatoslav N. Bagriantsev

Sci. Adv., **9** (37), eadi4147.
DOI: 10.1126/sciadv.adi4147

Science Advances (ISSN) is published by the American Association for the Advancement of Science. 1200 New York Avenue NW, Washington, DC 20005. The title *Science Advances* is a registered trademark of AAAS.

Science Advances
AAAS

Supplementary Materials for

3D architecture and a bicellular mechanism of touch detection in mechanosensory corpuscle

Yury A. Nikolaev *et al.*

Corresponding author: Elena O. Gracheva, elena.gracheva@yale.edu; Sviatoslav N. Bagriantsev, slav.bagriantsev@yale.edu

Sci. Adv. **9**, eadi4147 (2023)
DOI: 10.1126/sciadv.adi4147

The PDF file includes:

Other Supplementary Material for this manuscript includes the following:

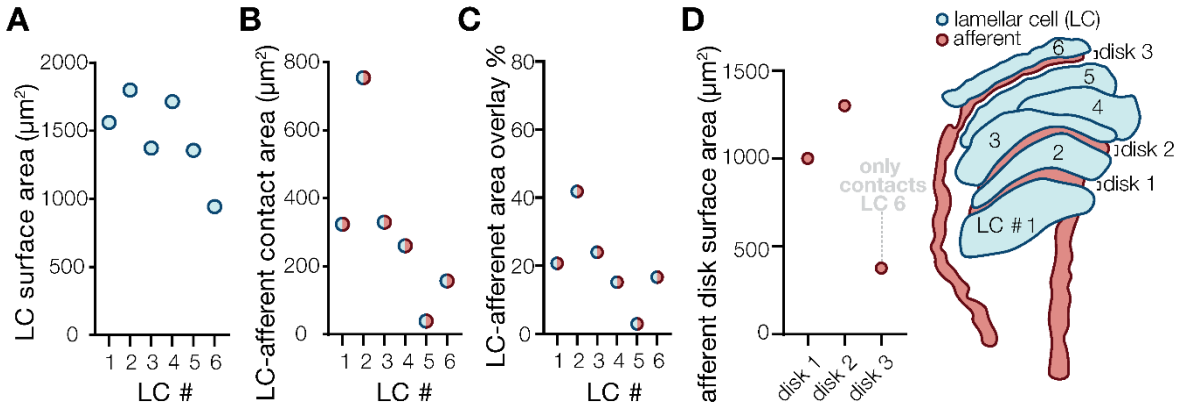

Fig. S1. Quantification of lamellar cell – afferent contact area. (A) Quantification of the surface area of lamellar cells in a reconstituted avian Meissner corpuscle. **(B**) Quantification of LC surface area in contact with the afferent. **(C)** Quantification of the portion of LC surface area in contact with afferents. **(D)** Quantification of afferent disk area in contact with LCs. The cartoon depicts a dually innervated corpsucle.

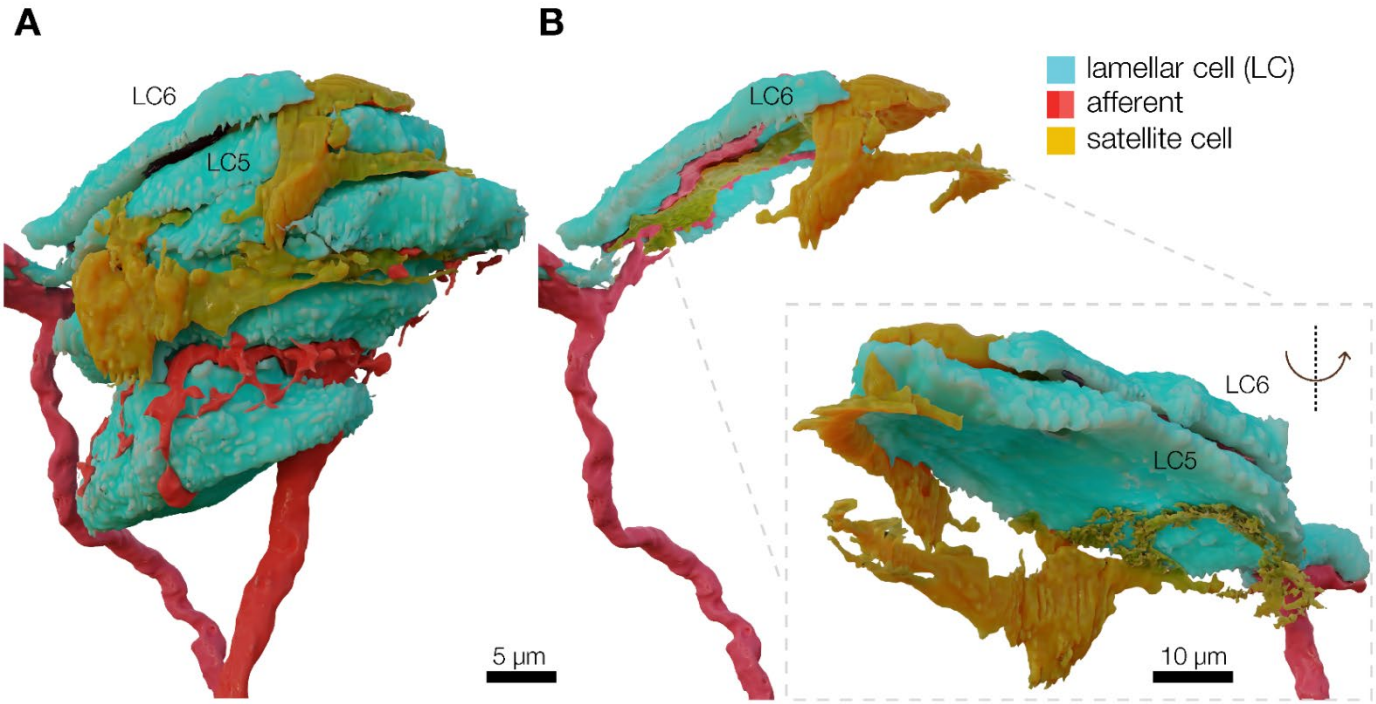

Fig. S2. Three-dimensional image of a satellite cell penetrating the core of avian Meissner corpuscle. (A) 3D reconstitution of the corpuscle core with a satellite cell. **(B)** Isolated 3D images of satellite cell projections relative to LCs and the afferent.

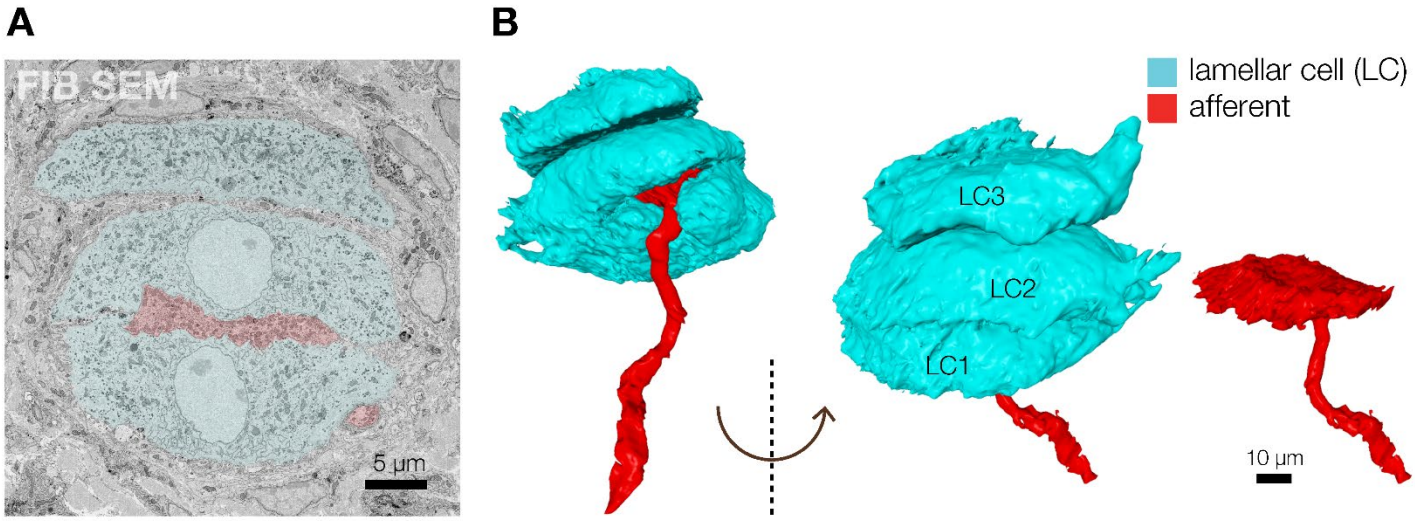

Fig. S3. Three-dimensional image of an avian Meissner corpuscle innervated by a single afferent. (A) A pseudo-colored FIB-SEM image of a section of a Meissner corpuscle in duck bill skin with three LCs (blue) innervated by a single afferent (red). **(B)** Partial 3D reconstruction of a Meissner corpuscle core (without satellite cells) innervated by a single afferent. The afferent (red) forms a single disc positioned between LC1 and LC2 (blue).

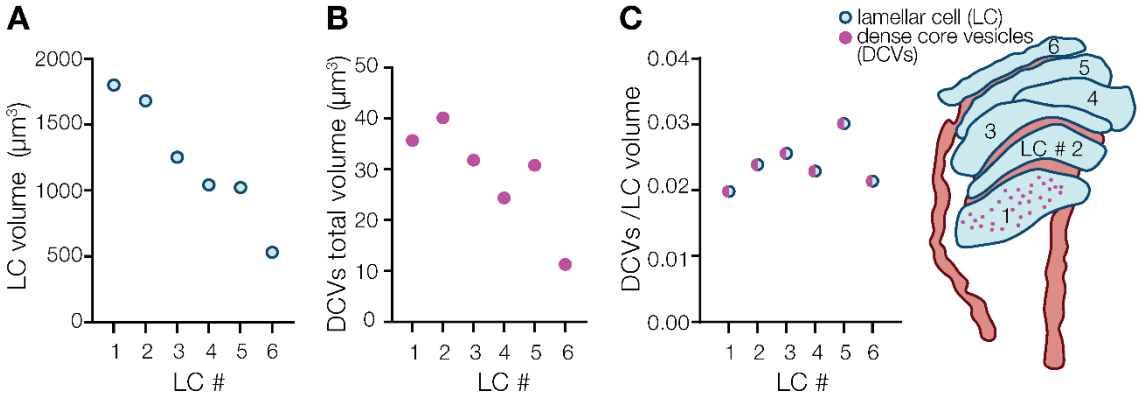

Fig. S4. Quantification of dense core vesicle size and volume. (A) Quantification of the lamellar cell volume. **(B)** Quantification of the volume occupied by dense core vesicles (DCV) in lamellar cells (LC). **(C)** Quantification of total DCV volume per LC. The cartoon depicts a dually innervated corpsucle.

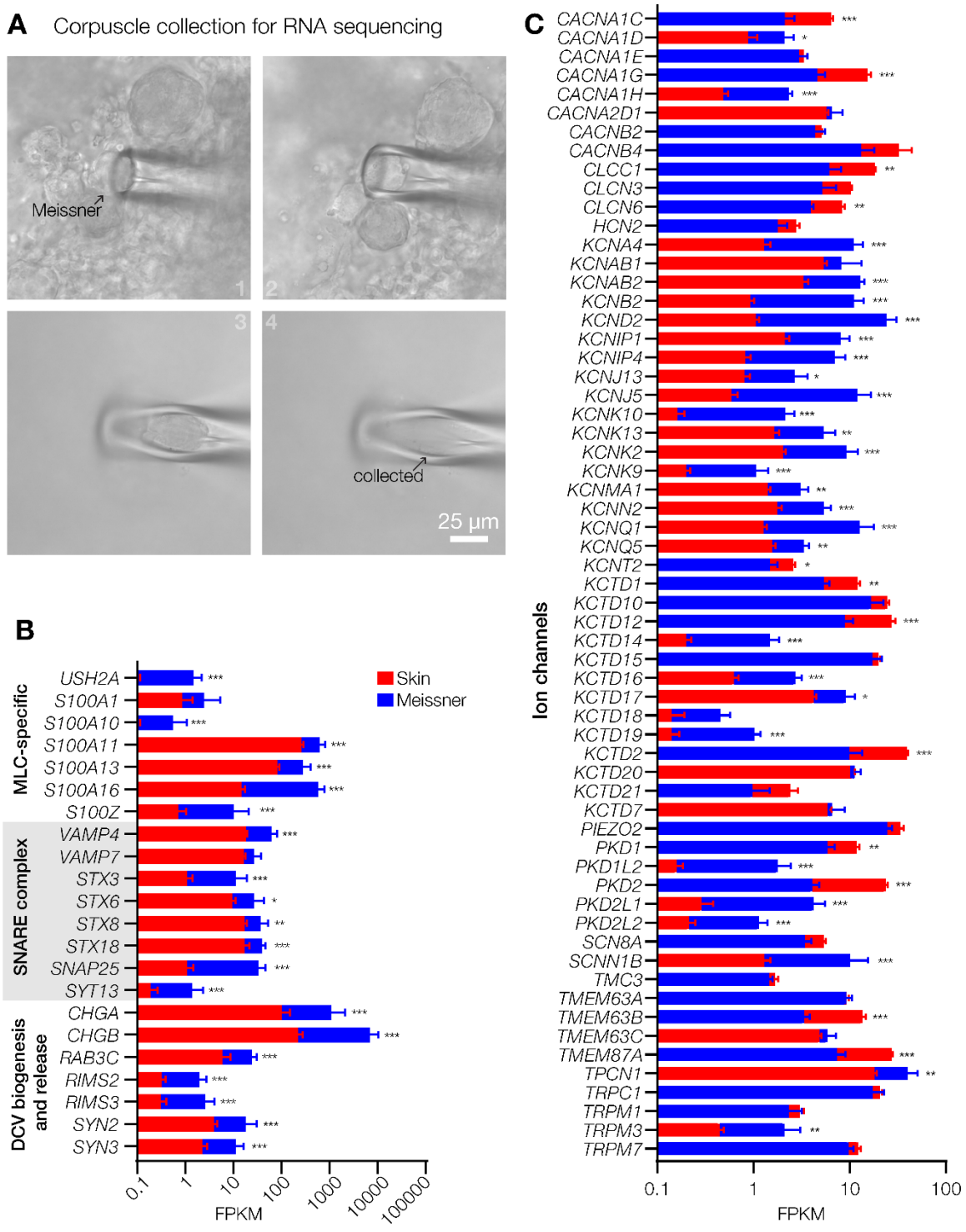

Fig. S5. RNA-sequencing of avian Meissner corpuscles. (A) Images of a Meissner corpuscle in the process of extraction from duck bill skin into a glass pipette for RNA sequencing. **(B, C)** Quantification of transcript levels in Meissner corpuscles and adjacent skin areas. Data are mean ± SEM from 6 corpuscles and 5 skin samples. FPKM, fragments per kilobase of exon per million mapped fragments. Statistics: quasi-likelihood F-test, **P* < 0.05, ***P* < 0.01, ****P* < 0.001.

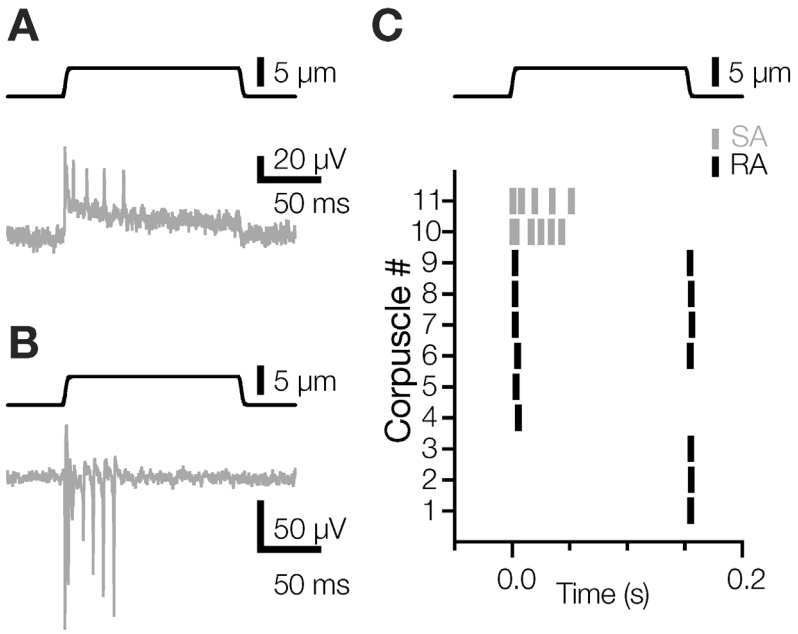

Fig. S6. Slowly and rapidly adapting responses in the afferents from avian Meissner corpuscles. (A, B) Recordings of action potentials in the afferent in response to mechanical stimulation. **(C)** Raster plot of two slowly adapting afferents (SA) and representative rapidly afferents (RA) from different corpuscles in response to mechanical stimulation.

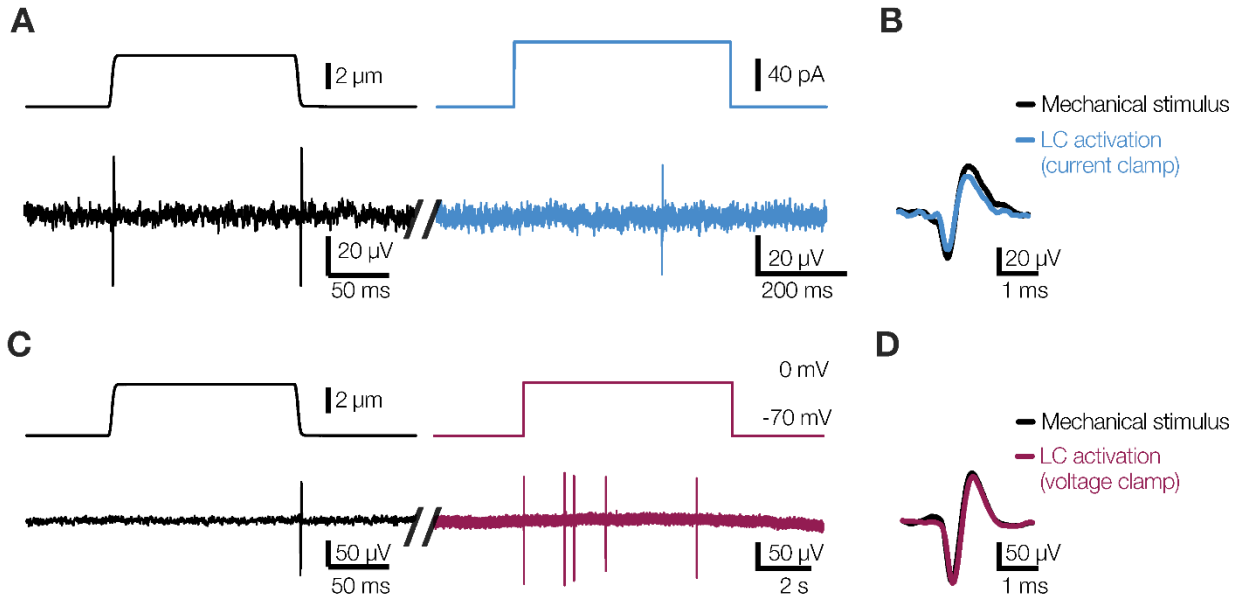

Fig. S7. Action potentials evoked in the afferent by mechanical stimulation or electrical activation of a single LC are indistinguishable. (A) Exemplar traces recorded in a Meissner afferent in response to mechanical stimulation of the corpuscle (left) or LC activation by current injection in the current clamp mode (right). **(B)** Overlay of APs evoked by mechanical stimulation or LC activation by current injection. **(C)** Exemplar traces recorded in a Meissner afferent in response to mechanical stimulation of the corpuscle (left) or LC activation by depolarization in the voltage clamp mode (right). **(D)** Overlay of APs evoked by mechanical stimulation or LC activation by depolarization.

Supplementary Table I. Accuracy statistics of FIB-SEM data segmentation for a Meissner corpuscle innervated by two afferents.

Object	IoU*	F1 score
Afferents	0.67	0.80
DCVs	0.80	0.89
Lamellar cells	0.99	0.99
Satellite cells	0.97	0.98
Collagen	0.94	0.97

**Intersection over Union*

Movie S1. 3D architecture of a duck Meissner corpuscle innervated by two afferents obtained using FIB-SEM.

Movie S2. 3D architecture of a duck Meissner corpuscle innervated by two afferents obtained using FIB-SEM. This is a non-rendered movie version depicting dense core vesicles (dark blue) inside lamellar cells.

Movie S3. An image stack of a fragment of lamellar cell-afferent contact area obtained by transmission electron microscopy tomography. The video shows a cross-section of the afferent disk sandwiched between two dense core vesicle-containing lamellar cells.

Movie S4. 3D reconstruction of a fragment of lamellar cell-afferent contact area obtained by transmission electron microscopy tomography. Shown are mitochondria (yellow), dense core vesicles (red), lamellar cell membrane (dark blue), afferent membrane (purple), clear vesicles (light blue), caveolae (green), membrane densities resembling adherens junctions (orange).

Movie S5. A close-up 3D reconstruction of a fragment of lamellar cell-afferent contact area obtained by transmission electron microscopy tomography, depicting fusing dense core vesicles, a caveolae, and tethers connecting lamellar cell and afferent membranes.